Research paper

Mesoporous TiO$_2$ films coated on carbon foam based on waste polyurethane for enhanced photocatalytic oxidation of VOCs

Xufang Qian[a], Meng Ren[a], Dongting Yue[a], Yao Zhu[a], Yu Han[a], Zhenfeng Bian[b], Yixin Zhao[a],*

[a] School of Environmental Science and Engineering, Shanghai Jiao Tong University, 800 Dongchuan Rd., Shanghai 200240, China
[b] The Education Ministry Key Lab. of Resource Chemistry, Shanghai Key Laboratory of Rare Earth Functional Materials, Shanghai Normal University, Shanghai 200234, China

ARTICLE INFO

ABSTRACT

Carbon foams (CFs) were prepared by using waste polyurethane foams (PUFs) as hard templates and phenolic resin as a carbon source. The obtained CFs were treated to be hydrophilic with plenty of carboxyle group by a wet oxidization method. Mesoporous TiO$_2$ films were then facilely deposited on hydrophilic carbon foams (hydro-CFs) because the hydrophilic carbon surface facilitates the formation of uniform coating layer. The macroporous hydro-CFs act as not only the supports of TiO$_2$ films but also the adsorbent for enriching the VOCs at the interface of hydro-CF and mesoTiO$_2$ films. The UV–vis and visible light irradiation photocatalytic oxidation of acetone and toluene was evaluated on mesoTiO$_2$/hydro-CF, which is higher than that of pure mesoTiO$_2$ and mesoTiO$_2$/CF. The mesoTiO$_2$/hydro-CF even showed visible light activity for acetone degradation due to the plausible carbon doping due to the strong interaction between the TiO$_2$ precursor and the hydro-CFs.

© 2017 Elsevier B.V. All rights reserved.

1. Introduction

Volatile organic compounds (VOCs) are the harmful gaseous pollutants in indoor and enclosed spaces such as train, aircraft cabin etc. [1,2]. The serious impact of indoor VOCs on human health and productivity has inspired the development of various technologies for VOCs elimination [3,4]. Photocatalytic oxidation of VOCs has been widely studied due to the merits of complete mineralization of pollutants into clean CO$_2$ and H$_2$O without second pollution [5–12]. TiO$_2$ is the most widely used photocatalyst owing to its low cost, safety, high activity and stability [1,13–15]. The different TiO$_2$ coating or coating with TiO$_2$ nanoparticles have been developed in applications of air purification, water treatment and self-cleaning etc. [16–22]. The coating technologies of TiO$_2$ films include sol-gel, liquid phase deposition, atomic layer deposition (ALD), chemical vapour deposition [20,23–25]. Strong adherence between Ti precursor (TiO$_2$ nanoparticles) and substrate is very important for obtaining a uniform TiO$_2$ coating or particle deposition layer. Normally, smooth and hydrophilic surfaces such quartzes, glass and steel were beneficial for deposition of uniform TiO$_2$ films [18,26,27].

However, the external surface area of the above skeleton was very limited for supporting TiO$_2$ films, while thick and condense TiO$_2$ films were detrimental for mass transformation and diffusion. Usually, only the several micrometer thick top TiO$_2$ films are effective for utilizing the photon [28]. Thus hierarchical skeletons with macroporous structures were desired for supporting TiO$_2$ photocatalysts [29]. Normally, macroporous structured materials were fabricated by using colloidal crystals and/or inverse opals as hard templates which were then removed by acid/base etching or thermal combustion methods [30–32].

Polyurethane foam (PUF) is one of the most widely used thermoset polymers for insulation, construction, transportation, decoration [33]. The specific PUF market was valued at 46.8 billion in 2014, which is expected to reach 72.2 billion by 2020 [34]. Normally, the treatment of the used and waste PUFs is landfill or incineration. The thermosetting polymer waste PUFs is difficult to be recycled. Accordingly, the reuse of PUFs waste is very urgent to relieve the environmental burden. On the other hand, the macroporous structure of PUFs has been well replicated after the coating process.

In this paper, carbon foams (CFs) were prepared using PUF as a hard template and phenolic resin as a carbon source. The obtained carbon foams were wet oxidized to generate oxygen containing groups (i.e. carboxyl). Mesoporous TiO$_2$ films were uniformly

coated on the hydrophilic carbon foams by a self-assembly sol-gel method. The mesoporous TiO_2 film decorated hydrophilic carbon foams showed enhanced photocatalytic oxidation activity for VOCs under UV–vis and visible light irradiation.

2. Experiment

2.1. Chemicals

Poly(propyleneoxide)-block-poly(ethyleneoxide)-block-poly(propyleneoxide) triblock copolymer Pluronic P123 ($PEO_{20}PPO_{70}PEO_{20}$, Mw = 5800) was purchased from Sigma-Aldrich. Sodium hydroxide (NaOH, ≥96%), hydrochloric acid (HCl, 36.0–38.0 wt%), $TiCl_4$, tetrabutyl titanate ($Ti(OBu)_4$), formalin solution (HCHO, 37.0–40.0 wt%), phenol were obtained from Shanghai Lingfeng Chemical Reagent Co., Ltd. Ammonium persulfate (($NH_4)_2S_2O_8$, ≥98.5 wt%), sulfuric acid (H_2SO_4, 95–98 wt%), ethanol, acetone and toluene were of analytical purity and were used as received. All of them were purchased from Sinopharm Chemical Reagent Co., Ltd.

2.2. Materials synthesis

2.2.1. Synthesis of carbon foams (CFs)

CFs were prepared by immersing waste PUF into phenolic resin ethanol solution followed by polymerization and carbonization in N_2 atmosphere. In a typical synthesis, 1.2 g phenolic resin was dissolved in 4.8 g ethanol to obtain a viscous solution. The gel was then coated on a PUF ($3 \times 3 \times 4$ cm^3), which was evaporated in air overnight before thermal polymerization at 100 °C for 24 h in oven. Pristine CFs were obtained after carbonization at 900 °C for 2 h in N_2 atmosphere.

2.2.2. Wet oxidation of CFs

Pristine CFs were treated by a mild wet oxidation method using ($NH_4)_2S_2O_4$ H_2SO_4 (APS) solution as an oxidant [35]. In a typical run, two cubic pristine CFs (around 1.0 g) were put in a wide-mouth flask containing a 60 mL 1.0 M APS solution (prepared in 2 M H_2SO_4). The above solution with pristine CFs was heated at 60 °C for 12 h in the presence of weak turbulence by stirring. The cubic CFs were washed by copious amounts of water and ethanol before drying in vacuum oven at 40 °C overnight to obtain the hydrophilic CFs (hydro-CFs).

2.2.3. Deposition of mesoporous TiO2 films

Mesoporous TiO_2 films were deposited on pristine CF and hydro-CFs by an evaporation induced self-assembly (EISA) method following by a hydrolysis-condensation process at 40 °C with humidity. For a typical synthesis, 1.0 g P123 was dissolved in 6.0 g ethanol to obtain a crystalline solution, then 1 mL $TiCl_4$ and 3 mL Tetrabutyltitanate was added drop-wise, respectively. The above viscous solution was deposited on pristine CF or hydro-CFs. The as-prepared composites were treated at 350 °C for 5 h with a heating rate of 1 °C/min, then the temperature increased to 550 °C (heating rate of 1 °C/min) and kept for 1 h. The obtained composites were designated as mesoTiO$_2$/CF and mesoTiO$_2$/hydro-CF, respectively.

2.3. Characterization

Powder XRD patterns were recorded on a Shimadzu XRD-6100 diffractometer with Cu Kα radiation. The data were recorded at a scan rate of 10°/min. Field-emission scanning electron microscopy (FESEM) measurements were performed on a JSM-7800F Prime scanning electron microscope. Fourier transform infrared (FTIR) spectra of the samples were measured on Tensor 27 FTIR spectrometer (Nicolet6700). Samples were diluted with KBr and compressed into thin pellets. N_2 adsorption-desorption isotherms were measured at 77 K with Quantachrome NOVA 4000e analyzer. The Brunauer-Emmett-Teller (BET) method was utilized to calculate the specific surface areas (SBET). The pore volumes and pore size distributions were derived from the adsorption branches of isotherms using the Barrett-Joyner-Halenda (BJH) model. Surface electronic states were analyzed by XPS (Perkin–Elmer PHI 5000C, AlKa). All binding energies were calibrated by using the contaminant carbon (C 1s = 284.6 eV) as a reference. Before adsorption measurements, all of samples were degassed in vacuum at 200 °C overnight. Gravimetric adsorption equilibrium analyses of benzene and toluene were carried out using a fully automated digital microbalance equipped with a vapor generator and connected to a high-vacuum system (Hiden Isochema Instrument, model IGA-002). Before measurements, all of samples were degassed in vacuum at 300 °C overnight. The measurements of saturated adsorption amounts of toluene were recorded on Thermogravimetric analyses (Mettler Toledo TGA-SDTA851 analyzer, Switzerland) in N_2 atmosphere (20 mL min^{-1}). The heating program underwent the following two steps: first with a heating rate of 20 °C min^{-1} up to 200 °C and maintenance at the same temperature for 3 h to remove non-adsorbed toluene; second with a heating rate of 5 °C min^{-1} up to 700 °C. It should be mentioned that the colors of the samples were white after TG analyses in N_2 atmosphere implying the desorption of toluene after the above heating program.

2.4. Photocatalytic degradation of VOCs

Photocatalytic degradation of gaseous VOCs were performed under UV–vis and visible light irradiation with a 420 nm cut filter using 500 W xenon lamp (CEL-HXF300). The concentrations of O in CFs were determined using the CHNS/O Analyzer (PerkinElmer, 2400 II). The distance of light source to the window of reactor is 2 cm (~380 mW/cm^2). A self-developed pryrex reactor (total volume of 250 mL) with a flat quartz window on the top was used, wherein 0.1 g of composite photocatalyst was placed in the bottom of the reactor. The reactor were sealed and flushed with O_2 for 30 min, and then 5 μL of liquid acetone (or toluene) were injected into the reactor and vaporized into gas phase. Before the lamp was switched on, the gas-solid adsorption equilibrium reached after 30 min. The photocatalytic oxidation of VOCs were evaluated by CO_2 detection at different time interval on gas chromatography (GC7900 equipped with a flame ionization detector (FID) & methane reforming furnace).

3. Results and discussions

Carbon foams (CFs) were prepared by coating phenolic resin precursor on PUF with dimensional size of $3 \times 3 \times 4$ cm^3, which followed by thermal polymerization at 100 °C and carbonization at 900 °C in N_2 (Fig. 1a–c). The final dimensional size of CF block is measured to be $1.8 \times 1.8 \times 2.4$ cm^3. The volumetric shrinkage ratio is about 78.4%. Mesoporous TiO_2 films was coated on a hydro-CF, wherein hydro-CF serves as a rigid skeleton for supporting meso TiO_2 films (Fig. 1c and d).

In order to obtain a uniform TiO_2 coating, pristine CF was treated by a wet oxidation process to be hydrophilic. The oxygen content of hydro-CF is measured to be 16.3 wt%, which is much higher than pristine CF (9.7 wt%). FTIR spectra of pristine CF and hydro-CF show an obvious band at 1720 cm^{-1}, which can be assigned to the stretching vibration of carboxyl groups. Additionally, several bands appear both for pristine CF and hydro-CF (Fig. S1). The bands at 1579 cm^{-1} can be ascribed to the vibration stretching of carbonyl and/or phenolic ring. Two bands at 1228 cm^{-1} and 1005 cm^{-1} result from the vibration stretching of C—O bonds. TG curve of
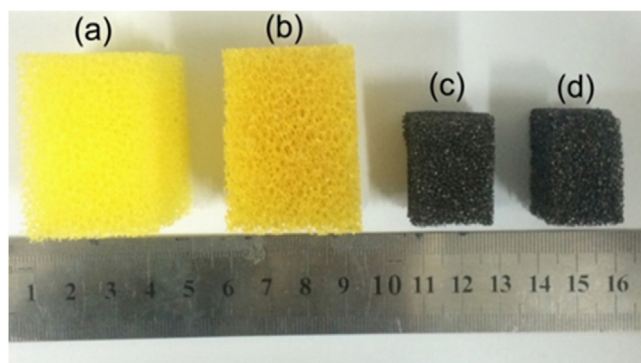
Fig. 1. Photographs of PUF (a), PUF coated with phenolic resin (b), hydro-CF (c), mesoTiO$_2$/hydro-CF (d).
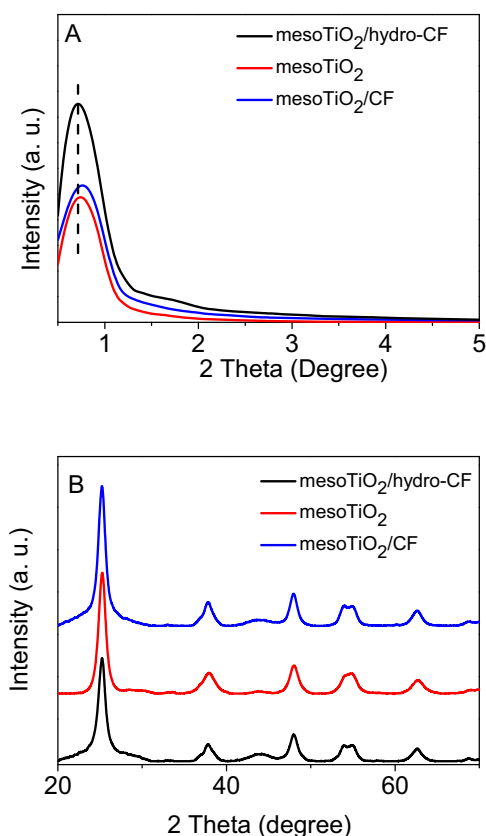
Fig. 2. Small angle and wide angle XRD patterns of mesoTiO$_2$/hydro-CF, pure mesoTiO$_2$, and mesoTiO$_2$/CF.

mesoTiO$_2$/CF shows two weight loss in the temperature ranges of 30–110 °C and 430–750 °C, which correspond to the evaporation of surface absorbed small molecules and the carbonization of pristine CF support (Fig. S2A). In comparison with mesoTiO$_2$/CF, mesoTiO$_2$/hydro-CF displays three weight loss steps at temperature ranges of 30–110 °C, 240–480 °C and 480–750 °C (Fig. S2B). A new weight loss step at 240–480 °C is ascribed to the decomposition of surface functional groups and small carbonaceous species. The weight percentage of mesoporous TiO$_2$ supported on pristine CF and hydro-CF are 46% and 76%, respectively, which reflects that the hydro-CF facilitates the deposition of TiO$_2$ films.

Small angle XRD pattern of pure mesoporous TiO$_2$ shows an obvious diffraction peak at 0.75, which indicates the mesostructure with poor ordering (Fig. 2A) [36]. With the supports of pristine CF, the diffraction peak is located at 0.76, which shows negligi-
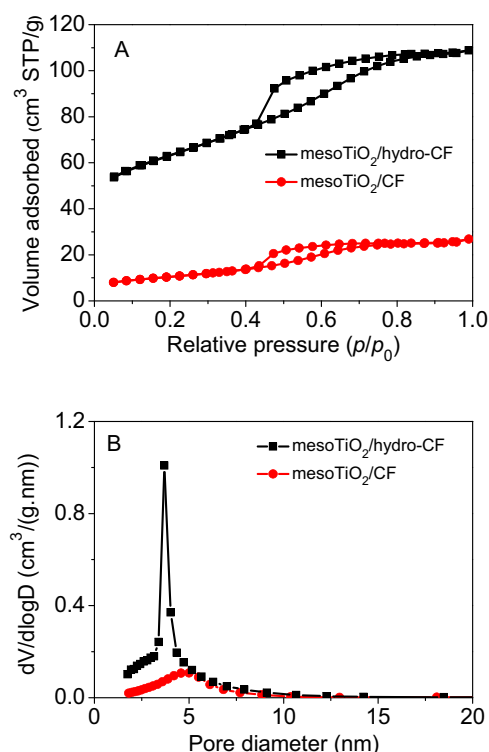
Fig. 3. N$_2$ sorption isotherms and pore size distributions of mesoTiO$_2$/hydro-CF and mesoTiO$_2$/CF.

Table 1
Textural properties of different materials.

Sample	S$_{BET}$ (m^2/g)	V$_t$ (cm^3/g)	Pore size (nm)
mesoTiO$_2$	106	0.12	5.4
mesoTiO$_2$/CF	37	0.04	4.8
mesoTiO$_2$/hydro-CF	210	0.14	3.4

ble effect of pristine CF on the TiO$_2$ films. However, the diffraction peak of mesoTiO$_2$@hydro-CF shifts to a low value of 0.71°, which should be attributed to the small shrinkage during heat treatment due to the strong interaction between TiO$_2$ and the hydro-CF support (Fig. 2A) [37]. Wide angle XRD patterns show the characteristic diffraction peak at 25, 38, 48 and 54° indexing to the (101), (004), (200) and (211) planes of anatase TiO$_2$ (Fig. 2B). The crystal sizes of TiO$_2$ nanocrystals for pure mesoTiO$_2$, mesoTiO$_2$/CF and mesoTiO$_2$/hydro-CF calculated by Scherrer's equation are 10.9, 10.8 and 12.9 nm, respectively. These results indicate that the hydro-CF support facilitates the crystallization of TiO$_2$ which may attribute to the large amount of carboxyl groups.

Nitrogen sorption isotherms of mesoTiO$_2$/CF and mesoTiO$_2$/hydro-CF (Fig. 3A) show the characteristic type-IV curves with H1 hysteresis loops, which are typical features of mesoporous structure. A much obvious capillary condensation step at relative pressure of 0.43–0.80 was observed for mesoTiO$_2$/hydro-CF, which corresponds to a narrow pore size distribution with a mean value of 3.7 nm. The pore size distribution of mesoTiO$_2$/CF is broad with a mean value of 4.8 nm. It means the mesostructure of TiO$_2$ films deposited on hydro-CF is much more ordered than that deposited on pristine CF. The specific BET surface area (S$_{BET}$) and total pore volume (V$_t$) of different samples are listed in Table 1. Based on the texture properties, the S$_{BET}$, V$_t$ and pore size of pure mesoTiO$_2$ are calculated to be 106 m^2/g, 0.12 cm^3/g and 5.4 nm, respectively. Owing to the hydrophobic properties of pristine CF with low specific surface area (Fig. S3), the
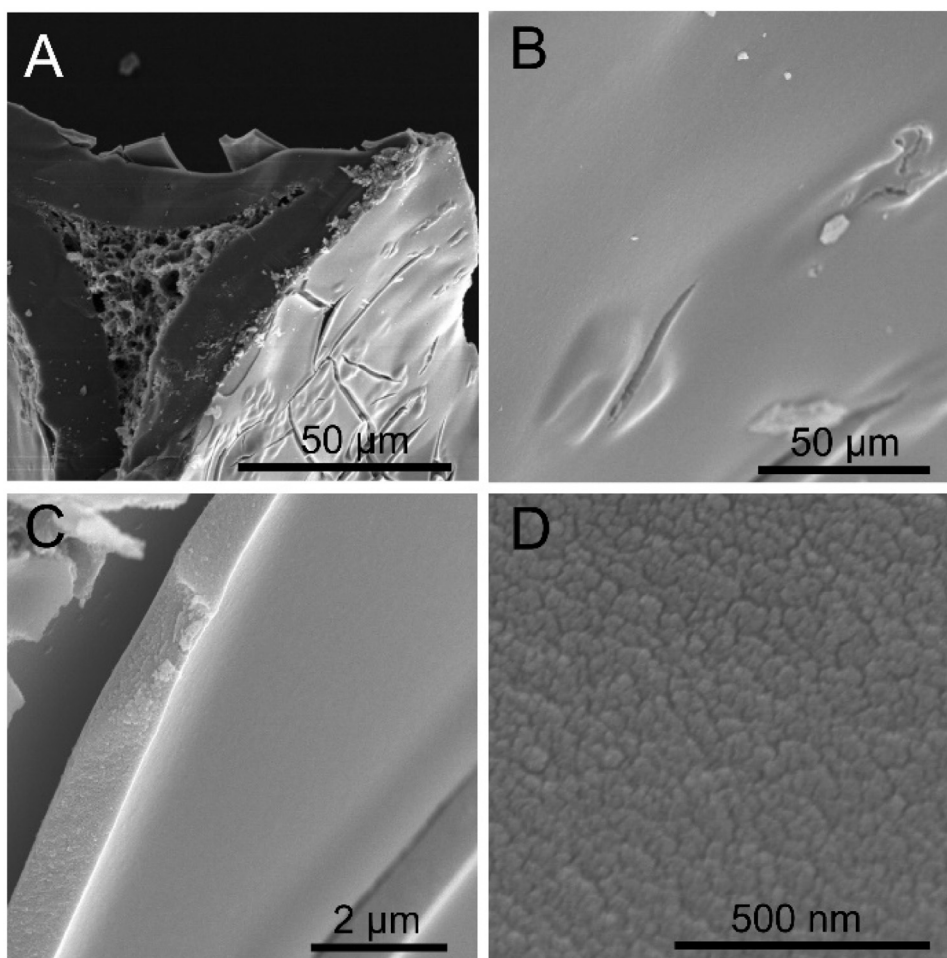
Fig. 4. SEM images of mesoTiO$_2$/hydro-CF: a, mesoTiO$_2$ films uniformly coated on hydro-CF skeleton; b, mesoTiO$_2$ surface with a crack; c, mesoTiO$_2$ film with thickness of 900 nm; d, high-resolution SEM image of mesoTiO$_2$ surface.

deposited mesoporous TiO$_2$ results in low S$_{BET}$, V$_t$ for mesoTiO$_2$/CF. In contrast, mesoTiO$_2$/hydro-CF shows greatly increased S$_{BET}$, and V$_t$, which can be attributed to the large weight percentage of TiO$_2$ films, a relatively small pore sizes (3.7 nm) and the contribution from hydro-CF.

SEM images of mesoTiO$_2$/hydro-CF show that uniform mesoporous TiO$_2$ films are homogeneously deposited on hydro-CF, although several cracks appear on the film due to the rough surface (Fig. 4a and b). The thickness of TiO$_2$ film is around 900 nm (Fig. 4c). High resolution SEM image displays compact film composed of TiO$_2$ nanocrystals (Fig. 4d). The corresponding EDX results indicate the presence of C, O Ti elements (Fig. S4). On the other hand, only some TiO$_2$ fragments with coarse surface are present on pristine CF skeleton indicating the unsuccessful coating of mesoporous TiO$_2$ films on the surface of CF skeleton (Fig. S5). The above phenomenon is in good consistence with the TGA results, in which the weight percentage of TiO$_2$ on pristine CF (46%) is almost half lower than the hydro-CF skeleton (76%).

The XPS spectra (Fig. S6) of mesoTiO$_2$/hydro-CF indicated it contains Ti, O, C elements. The binding energies of Ti 2p3/2 and Ti 2p1/2 locate at 459.3 eV and 464.9 eV, respectively (Fig. 5A). However, the spin-orbital splitting of Ti 2p3/2 and Ti 2p1/2 is 5.6 eV, which is smaller than that of pure mesoTiO$_2$ (5.8 eV) without hydro-CF supporting. The phenomenon could be attributed to the plausible C doping in mesoTiO$_2$/hydro-CF sample [38]. The high resolution C 1s XPS spectrum of mesoTiO$_2$/hydro-CF shows one main peak and shoulder peak at the binding energies of 284.8 eV and 286.5 eV,

respectively, which corresponds to the presence of C—C of hydro-CF support, C—O (and/or C=O) species (Fig. 5B). It should be mentioned that the peak at lower binding energy (242.4–241.4 eV) was not found indicating the absence of C—Ti bond [39,40] The above results reflect the possible substitution of the lattice titanium atoms with the formation of a Ti—O—C structure in mesoTiO$_2$/hydro-CF.

The gas-solid photocatalytic oxidation (PCO) of acetone and toluene was studied over photocatalysts mesoTiO$_2$@CF, mesoTiO$_2$/hydro-CF and pure mesoTiO$_2$ by evaluating the CO$_2$ production under UV–vis and visible light irradiation. As shown in Fig. 6A, the blank experiment without photocatalysts shows that the acetone is rarely degraded within 2 h, which indicates the acetone is very stable under UV–vis light irradiation. In the presence of the mesoTiO$_2$/CF, the time profile of CO$_2$ production shows gradually increased CO$_2$ production within 2 h. The CO$_2$ production rate in initial 60 min is 0.13 μmol/min. For mesoTiO$_2$/hydro-CF with uniform TiO$_2$ films, the initial CO$_2$ production rate increases to 0.18 μmol/min higher than the case of mesoTiO$_2$/CF. The initial CO$_2$ production rate on the control sample pure mesoTiO$_2$ is 0.14 μmol/min, a little higher than mesoTiO$_2$/CF due to the probably light shield effect by black carbon. The above results indicate that the uniform mesoporous TiO$_2$ films decorated on hydro-CF can effectively promote the photocatalytic degradation of gaseous polar acetone. The promotion effects come from the well-crystallized anatase nanocrystals, hydro-CF skeleton for adsorption of polar gaseous acetone and fast mass transportation within the hierarchical frameworks. On the other hand, the CO$_2$ production of
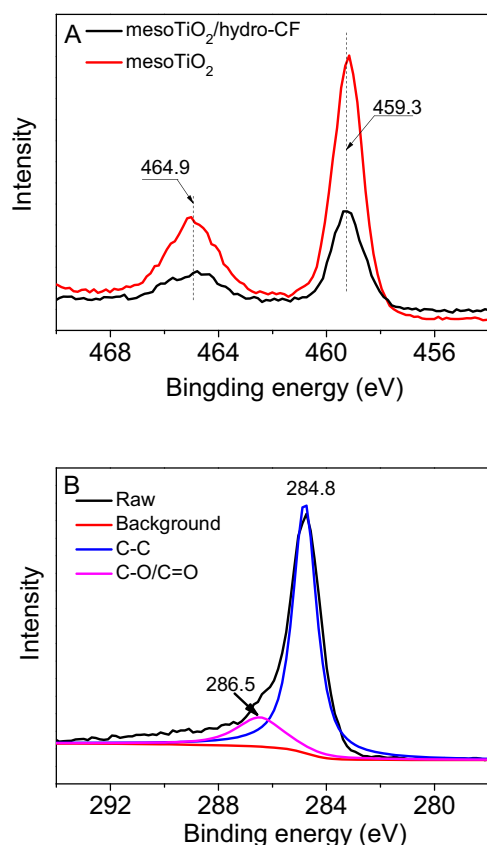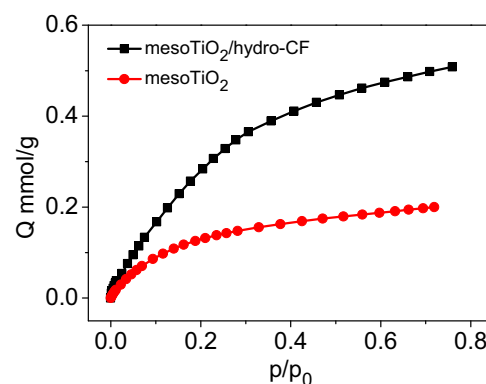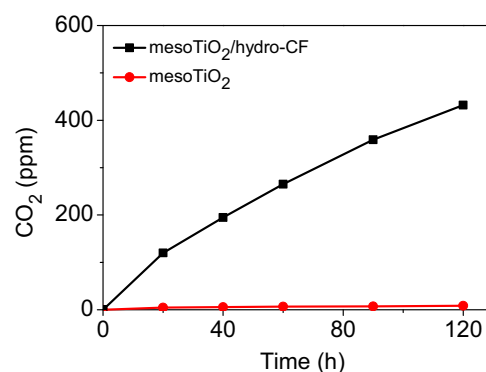
Fig. 5. XPS spectra of Ti 2p of $mesoTiO_2$/hydro-CF and $mesoTiO_2$ (A), and C 1s of $mesoTiO_2$/hydro-CF (B), respectively.
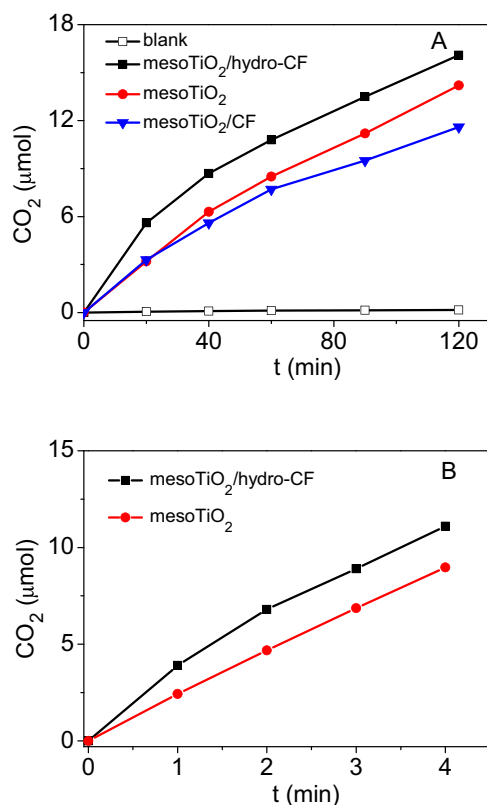
Fig. 6. CO_2 contents released during the PCO of acetone (A) and toluene (B) in the presence of different composite photocatalysts under UV–vis light irradiation.

Fig. 7. The adsorption isotherms of toluene vapor at 298 K on different materials.


Fig. 8. The amounts of CO_2 released during the PCO toluene under visible light irradiation ($\lambda > 420$ nm).

PCO of toluene over $mesoTiO_2$/hydro-CF and $mesoTiO_2$ shows that the presence of hydro-CF support could significantly enhance the mineralization efficiency of toluene under UV irradiation (Fig. 6B). To detect the adsorption behaviour of $mesoTiO_2$/hydro-CF and $mesoTiO_2$, we measured the adsorption isotherms of toluene at 298 K. The adsorption amount Q increased gradually with increasing the relative pressure, whereas the $mesoTiO_2$/hydro-CF shows more obvious adsorption increase than the pure $mesoTiO_2$ at the tested relative pressure (p/p_0) (Fig. 7). The total adsorption amount on $mesoTiO_2$/hydro-CF (0.5 mmol/g) is 2.5 times larger than that of pure $mesoTiO_2$ (0.2 mmol/g). The adsorption capacity of toluene measured by TG on $mesoTiO_2$/hydro-CF was 75 mg/g, which is 3 times larger than pure $mesoTiO_2$ (20 mg/g), which is in consistent with the IGA results. Accordingly, the hydro-CF support is also benefit for accumulation of organic gaseous molecules such as toluene with low polarity. The enhanced adsorption equilibrium is benefit for the photocatalytic oxidation of gaseous organic pollutants [28].

PCO of acetone was also evaluated under visible light ($\lambda > 420$ nm) irradiation (Fig. 8). It is obvious that the CO_2 was produced gradually on $mesoTiO_2$/hydro-CF while negligible CO_2 was produced on pure $mesoTiO_2$. The above results accompanying with the XPS results could be ascribed to C doped into $mesoTiO_2$ films.

PCO treatment of VOCs needs photocatalyst materials, while substrates usually become the good candidate for supporting powder photocatalyst material. Mass transfer of the VOCs from free gas phase to the solid phase plays an important role and also influence the degradation efficiency in gas phase PCO process. In the present work, we coated mesoporous TiO_2 films on hydro-CF which was produced from waste PUFs and phenolic resin. Hydro-CF with macroporous structures provides a large surface for depositing TiO_2 than glass (and/or stainless steel) plates, and also facilitates the accumulation of VOCs at the interface of TiO_2 and hydro-CF. The
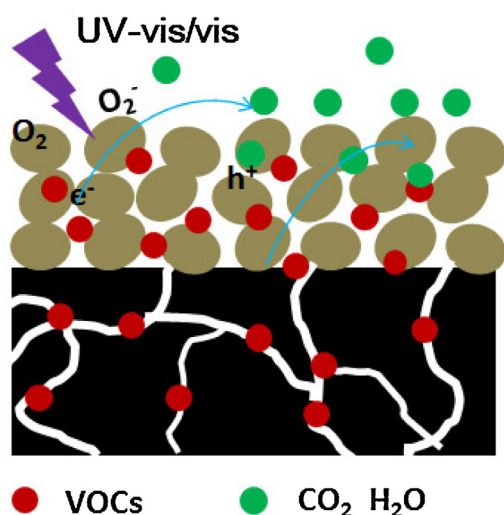
Fig. 9. The proposed photocatalytic oxidation of VOCs in O_2 under UV–vis and visible light irradiation for mesoTiO$_2$/hydro-CF.

schematic illustration of PCO of VOCs upon mesoTiO$_2$/hydro-CF composite was shown in Fig. 9. MesoTiO$_2$ films can be excited to form e$^-$/h$^+$ pairs under UV–vis and visible light irradiation. The h$^+$ is one of the strong oxidant for gaseous VOCs mineralization. On the other hand, hydro-CF substrate can effectively adsorb the VOCs molecules which increases the concentration of VOCs at the interfacial between mesoTiO$_2$ and hydro-CF substrate, as well as facilitate the mass transfer of VOCs due to the macroporous structure.

4. Conclusions

Mesoporous TiO$_2$ films were uniformly deposited on hydro-CF using waste PUF as a hard template and phenolic resin as a carbon source. The combination of mesoTiO$_2$ photocatalyst and hydro-CF facilitated mass transfer and the accumulation of VOCs at the interfacial of photocatalyst and substrate. Photocatalytic oxidation of acetone and toluene indicated that the degradation activity of mesoTiO$_2$/hydro-CF is higher than that of pure mesoTiO$_2$ and mesoTiO$_2$/CF. Carbon atom doping into mesoporous TiO$_2$ films was found which endowed visible light responsive activity for PCO degrading of acetone. In summary, hydro-CF prepared by waste PUF and phenolic resin provided a good candidate for supporting TiO$_2$ photocatalyst in application of indoor air treatment.

Acknowledgments

Appendix A. Supplementary data

Supplementary data associated with this article can be found, in the online version, at http://dx.doi.org/10.1016/j.apcatb.2017.04.059.

References

[1] Y. Boyjoo, H. Su, J. Liu, V.K. Pareek, S. Wang, Chem. Eng. J. 310 (2017) 537–559.
[2] S. Wang, H.M. Ang, M.O. Tade, Environ. Int. 33 (2007) 694–705.
[3] A.H. Mamaghani, F. Haghighat, C.-S. Lee, Appl. Catal. B: Environ. 203 (2017) 247–269.
[4] I. Dhada, P.K. Nagar, M. Sharma, N. Gupta, Environ. Eng. Sci. 33 (2016) 970–977.
[5] X. Qian, D. Yue, Z. Tian, M. Reng, Y. Zhu, M. Kan, T. Zhang, Y. Zhao, Appl. Catal. B: Environ. 193 (2016) 16–21.
[6] W. Donphai, T. Kamegawa, M. Chareonpanich, K. Nueangnoraj, H. Nishihara, T. Kyotani, H. Yamashit, Phys. Chem. Chem. Phys. 16 (2014) 25004–25007.
[7] H. Huang, H. Huang, Q. Feng, G. Liu, Y. Zhan, M. Wu, H. Lu, Y. Shu, D.Y.C. Leung, Appl. Catal. B: Environ. 203 (2017) 870–878.
[8] J. Lyu, J. Gao, M. Zhang, Q. Fu, L. Sun, S. Hu, J. Zhong, S. Wang, J. Li, Appl. Catal. B: Environ. 202 (2017) 664–670.
[9] A. Suligoj, U.L. Stanger, A. Ristic, M. Mazaj, D. Verhovsek, N.N. Tusar, Appl. Catal. B: Environ. 184 (2016) 119–131.
[10] S. Weon, W. Choi, Environ. Sci. Technol. 50 (2016) 2556–2563.
[11] J. Mo, Y. Zhang, Q. Xu, Y. Zhu, J.J. Lamson, R. Zhao, Appl. Catal. B: Environ. 89 (2009) 570–576.
[12] Y. Boyjoo, H. Sun, J. Liu, V.K. Pareek, S. Wang, Chem. Eng. J. 310 (2017) 537–559.
[13] R. Asahi, T. Morikawa, T. Ohwaki, K. Aoki, Y. Taga, Science 293 (2001) 269–271.
[14] A. Fujishima, X. Zhang, D.A. Tryk, Surf. Sci. Rep. 63 (2008) 515–582.
[15] B. Qiu, M. Xing, J. Zhang, J. Am. Chem. Soc. 136 (2014) 5852–5855.
[16] Z. Bian, J. Zhu, H. Li, J. Photochem. Photobiol. C 28 (2016) 72–86.
[17] X. Qian, K. Fuku, Y. Kuwahara, T. Kamegawa, K. Mori, H. Yamashita, ChemSusChem 7 (2014) 1528–1536.
[18] S. Lorencik, Q.L. Yu, H.J.H. Brouwers, Chem. Eng. J. 306 (2016) 942–952.
[19] F. Montecchio, D. Chinungi, R. Lanza, K. Engvall, Appl. Surf. Sci. 283 (2017) 283–296.
[20] C. Piccirillo, C.J. Denis, R.C. Pullar, R. Binions, I.P. Parkin, J.A. Darr, P.M.L. Castro, J. Photochem. Photobiol. A 332 (2017) 45–53.
[21] J. Lyu, L. Zhu, C. Burda, Catal. Today 225 (2014) 24–33.
[22] X. Zhao, M. Liu, Y. Zhu, Thin Solid Films 515 (2007) 7127–7134.
[23] M. Brancher, D. Franco, H.d.M. Lisboa, Environ. Technol. 37 (2016) 2852–2864.
[24] B.A. Marinho, R.O. Cristovao, R. Djellabi, J.M. Loureiro, R.A.R. Boaventura, V.J.P. Vilar, Appl. Catal. B: Environ. 203 (2017) 18–30.
[25] S. Nikodemski, A.A. Dameron, J.D. Perkins, R.P. O'Hayre, D.S. Ginley, J.J. Berry, Sci. Rep. 6 (2016) 1–8.
[26] Z. Bian, F. Cao, J. Zhu, H. Li, Environ. Sci. Technol. 49 (2015) 2418–2424.
[27] L. Hurtado, D. Solis-Casados, L. Escobar-Alarcon, R. Romero, R. Natividad, Chem. Eng. J. 304 (2016) 39–47.
[28] C.S. Lugo-Vega, B. Serrano-Rosales, H. de Lasa, Appl. Catal. B: Environ. 198 (2016) 211–223.
[29] L. Zhang, Z. Xing, H. Zhang, Z. Li, X. Wu, X. Zhang, Y. Zhang, W. Zhou, Appl. Catal. B 180 (2016) 521–529.
[30] T. Kamegawa, Y. Ishiguro, H. Seto, H. Yamashita, J. Mater. Chem. A 3 (2015) 2323–2330.
[31] G.S. Shao, X.J. Zhang, Z.Y. Yuan, Appl. Catal. B 82 (2008) 208–218.
[32] J. Yu, L. Zhang, B. Cheng, Y. Su, J. Phys. Chem. C 111 (2007) 10582–10589.
[33] P.K.S. Pillai, S. Li, L. Bouzidi, S.S. Narine, Ind. Crops Prod. 83 (2016) 568–576.
[34] S. Farhan, R. Wang, H. Jiang, K. Li, Mater. Des. 101 (2016) 332–339.
[35] Z. Wu, P.A. Webley, D. Zhao, Langmuir 26 (2010) 10277–10286.
[36] Z. Bian, J. Zhu, S. Wang, Y. Cao, X. Qian, H. Li, J. Phys. Chem. C 112 (2008) 6258–6262.
[37] X. Qian, J. Du, B. Li, M. Si, Y. Yang, Y. Hu, G. Niu, Y. Zhang, H. Xu, B. Tu, Y. Tang, D. Zhao, Chem. Sci. 2 (2011) 2006–2016.
[38] W. Wei, C. Yu, Q. Zhao, G. Li, Y. Wan, Chem. Eur. J. 19 (2013) 565–576.
[39] W. Ren, Z. Ai, F. Jia, L. Zhang, X. Fan, Z. Zou, Appl. Catal. B: Environ. 69 (2007) 138–144.
[40] S.U.M. Khan, M. Al-Shahry, W.B. Ingler, Science 297 (2002) 2243–2245.